Received: 21 February 2024 | Revised: 22 April 2024 | Accepted: 24 April 2024

DOI: 10.1002/pen.26781

RESEARCH ARTICLE

POLYMER ENGINEERING AND SCIENCE WILEY

An experimental-based thermal prediction model for butt fusion welding of polymer pipes

Walid Awadi[1,2] | **Mondher Zidi**[1] | **Maher Ben Chiekh**[3]

[1]University of Monastir, National Engineering School of Monastir (ENIM), Laboratory of Mechanical Engineering (LGM), Monastir, Tunisia

[2]Higher Institute of Technological Studies of Jendouba, Jendouba North, Tunisia

[3]University of Monastir, National Engineering School of Monastir (ENIM), Laboratory for the the Study of Thermal and Energy Systems (LESTE), Monastir, Tunisia

Correspondence
Maher Ben Chiekh, ENIM, Laboratory for the Study of Thermal and Energy Systems LESTE, University of Monastir, LR99ES31, Monastir 5000, Tunisia.
Email: maher.benchiekh@enim.rnu.tn

Abstract

High-density polyethylene (HDPE) is one of the most used thermoplastic materials for piping applications, due to its significant advantages. The butt-fusion process is the most used joining processes for HDPE welding. During the process, the behavior of the material changes. This behavioral change depends on the applied welding process and on the used parameters. Thermal analysis can be used as a tool to reveal and evaluate the modifications of the physical and mechanical properties. In this study, an experimental program was applied to HDPE to assess the effects of different parameters on the welding process including heating temperature, heating duration and the applied strength. Tests are performed according to a full factorial design of experiment (DOE). Mathematical models derived from experimental data are used to establish relationships between the input parameters, such as force and heating duration and the corresponding outputs such as temperature distribution during the different welding phases and the thickness of the molten polymer. The empirical models can be used to implement a control strategy for the temperature and hence quantify the thickness of the molten zone to improve the quality of the weld joint by selecting the appropriate welding conditions for the molten zone.

Highlights

- High-density polyethylene piping butt-fusion joint examination using Infrared imaging.
- Spatial–temporal distribution of temperature for different phases of the welding process.
- Mathematical Regression techniques are performed.
- Thickness of molten polymer is assessed.
- Results are useful for saving material and improvement of the process.

Abbreviations: F_1, equalization force; F_2, heating force; F_4, welding force = $\mathbf{F_1}$; t_1, equalization time; t_2, heating time (variable); t_3, time of heating plate removal; t_4, welding time; t_5, cooling time; t_{ch}, heating duration (constant 30 s, 50 s or 70 s); $T_{exp,i}$, measured temperature; t_f, total duration of welding and cooling; $T_{pred,i}$, predicted temperature; C_p, specific heat, at constant pressure; DOE, design of experiment; EA, automated force tests; Fs, softening and welding force; HDPE, high-density polyethylene; N, sample size; PE, polyethylene; PN, nominal pressure; r, radius direction; SDR, standard dimension ratio; T, temperature; T_0, heating plate temperature; x, total displacement of the mobile jaw during the welding phase; Xf, pipe length of temperature study (20 mm); X_{fusion}, melting depth; α, thermal diffusivity; θ, circumferential direction; λ, thermal conductivity of the pipe; ρ, density.

KEYWORDS

butt-fusion welding, conduction heat transfer, high-density polyethylene, mathematical modeling, temperature distribution

1 | INTRODUCTION

Currently, a huge variety of products are designed and produced with polymers. High-density polyethylene (HDPE) is commonly used because of its significant cost and labor savings, strong resistance to corrosion, ability to withstand thermal and mechanical shocks, and ease of handling due to its light weight. HDPE pipes are currently used for public water and gas distribution. For these applications, joining the pipe's ends must be performed due to the important distances between installations.

Butt fusion, also known as heating plate fusion, is a widely used technique for effectively connecting the ends of pipes. A heated metal plate is used to heat and melt the ends of the thermoplastic parts. When the interfaces are sufficiently melted, the heating plate is removed, and the extremities are joined together because of the application of an axial load.

The use of the butt-welding technique is widely adopted as a method of joining high-density polyethylene (HDPE) pipes having a thickness of more than 2 mm. The technique is qualified as economical and simple. It also ensures hermetic welds with high strength and is valid for treating large and small parts. Welding parameters such as heating temperature, heating time, welding force (pressure), cooling time, existence of contaminants at weld interface, material homogeneity, and welding technician qualifications are the determining factors in the quality of the weld joint.[1–4]

Thermomechanical butt-welding of polymers has been reported in several papers in which, the factors influencing the process have been examined. All researchers concluded that temperature is the most important factor, while increasing pressure has a positive impact on weld strength. The impact of joining pressure on the welding of perpendicular beams made of different types of polypropylene was addressed by Gehde et al.[5] They concluded that while the joining pressure should be high enough to produce a good junction in the joining area, too high pressure in a bending test, could lead to cracks inside the joining area. Watson and Murch[6,7] investigated the process of welding plastics in the form of tanks made of polypropylene, polystyrene, or polyphenylene oxide. They found that the most significant parameters for obtaining good welds were those associated with the heating phase (heating time and heating plate temperature). Stokes and Conway[8] conducted research on standard polymer materials and they provided experimental measurements about weld strength and failure strain depending on heating plate temperature.

More recently, various experiments were conducted to assess the influence of the main process parameters, resulting in the development of mathematical models. These models capture the combined effect and interactions of selected parameters. Taguchi experimental design method was implemented by Ulker et al.[1] as a statistical design of experiment technique to investigate the influence of welding parameters in hot plate welding process of polycarbonate (PC)/acrylonitrile-butadiene-styrene (ABS) blends. They observed that plate temperature is the most influential parameter with a value of 51.1% on joint strength, followed by welding displacement of about 37% and heating time of about 10.5%. A multi-criteria decision-making approach was also used by Mathiyazhagan et al.[9] to assess the impact of 16 parameters associated with hot plate welding. The identification of causal relationships between evaluation criteria led to the conclusion that plate temperature and heating time were the most influential parameters.

The welding process comprises four phases,[10,11] represented in the diagram in Figure 1. In phase I, the parts are brought into contact with the heating plate, called equalization. A relatively high pressure (F1) is applied to ensure complete adaptation of the surfaces of the pipe and the tool. The hot tool conductively heats the ends of the work pieces, and the heat transfer causes the temperature to increase rapidly over time. Once the melting temperature of the plastic is reached, the melted material begins to flow. A small motion of the pipe is observed as melt front removes surface imperfections and deformations. During phase II, the melting pressure is reduced, allowing the additional heat to enter the material and the melt layer to thicken.

When a sufficient melting thickness is reached, the tool is removed (Phase III), and the pressure and the surface temperature drop. The duration of this tilting phase must be as short as possible (a few seconds) to avoid premature cooling of the molten material. A thin and solid "skin" will be formed on the joint interface if the time is too long, affecting the quality of the weld.

In phase IV, the parts are assembled under pressure, causing molten material to flow laterally outward while cooling and solidifying.

Heating the surfaces of the pipe in the molten state causes an increase in the thermal movement of the chains of the polymer (polyethylene) through the fusion

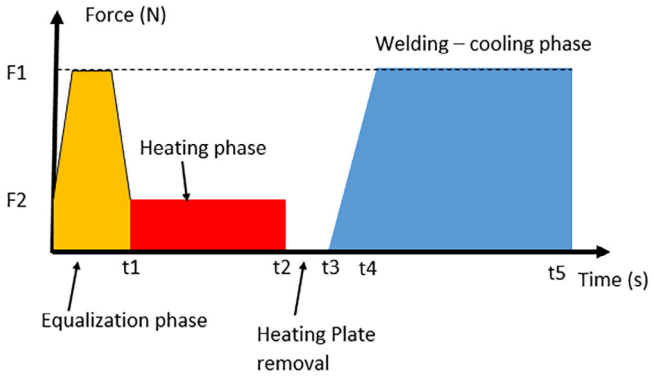

FIGURE 1 Pressure force vs. time curve showing the four phases of butt-fusion welding.

layer. When applying axial pressure to the two pipe extremities, the molecular chains from either side entangle under the mutual effects of thermal motion and pressure and remain entangled after cooling.[12,13] In the welding zone, the molten HDPE undergoes deformation, molecular interpenetration, and recrystallization, which leads to the formation of a new structure under the stress imposed by the welding process. During the recrystallization phase, applied stresses as well as thermally induced stresses are present on either side of the weld bead. The study of the process must be mastered to select the appropriate welding force; the aim of which is to have better mechanical characteristics and to minimize welding defects (lack of fusion[14]). Indeed, the application of an excessive force causes the refuge of all the molten polymer in the bead. This provokes the problem of the incomplete fusion.

In this research, the temperature distribution of the various welding phases at the weld bead is studied experimentally and modeled. The melted zone for the carefully selected stress is determined beforehand. Thermal analysis can be used as tool to reveal and to evaluate the modification of the physical and mechanical properties.

2 | METHODOLOGY

2.1 | Description of the experimental set-up

Experiments are performed on cross sections of PE100 pipe, manufactured by MedPlast Tunisia, having the following characteristics: 75 mm in diameter, 4.5 mm in thickness giving a surface-to-diagonal ratio SDR = 17, 250 mm in length and a nominal pressure equal to 10 MPa. This pipe model is largely used in the country mainly by public entities in the field of water distribution and agriculture. HDPE properties are given in Table 1. PE100 has a density of 0.96 g/cm^3.

TABLE 1 HDPE properties (including PE100).[15]

Density	0.941–0.967 g/cm^3
Glass transition T_g	−130°C
Melting temperature	128–137°C
Usual melt processing range	160–240°C
Thermal conductivity λ	0.4 W/(m.K) at 23°C and 0.25 W/(m.K) at 150°C
Heat capacity C_p	2200–2400 J/(Kg.K)
Enthalpy of fusion	210,000–300,000 J/Kg

Thermomechanical butt-fusion welding was carried out on a VIRAX D-40-160 mm machine. The corresponding procedure is outlined in the DIN – DVS 2207–1 guidelines for welding of thermoplastics specifically focusing on heated element welding of pipes, piping parts, and panels made out of polyethylene. The machine was converted into a fully automated machine using LabView after the incorporation of an electric cylinder to enable automatic movement and remote control of its mobile spindle. The experimental set-up requires an electric actuator, MYRIO card, power supply card, and two force and position sensors. Subsequently, the data from the various tests are checked, measured, and recorded.

Figure 2 shows different experimental phases of the welding process. First, we make sure there are no axial or radial offset defects. If so, both ends are milled until the defects are eliminated. Subsequently, the welding cycle is started by placing the heating plate between the two sections. The cycle begins with a softening phase followed by heating for a well-defined time. After the removal of the plate, the welding and cooling phase occurs.

The tests were carried out under the ambient conditions of the mechanical workshop of the Higher Institute of Technological Studies of Jendouba, Tunisia (ISETJ).

Real-time ambient conditions are measured using a thermos-hygrometer brand CHAUVIN ARNOUX. Mean values of humidity and temperature during the tests were 64.5% and 22.5°C, respectively. Simultaneously, infrared thermal images are recorded using an infrared thermal camera IR C.A 1886. The camera manufacturer indicates a measurement accuracy of around ±2°C.

2.2 | Full factorial DoE

There are several methods to efficiently design experiments.[16] Among these methods, the full factorial DoE considers all possible combinations within the experimental space. Generally, full factorial designs are expensive but not for a small number of studied parameters. Three parameters (heating duration, heating plate temperature, and controlled forces) are addressed, and the full factorial DoE was used to capture first and second order interactions. Table 2 gives the values of the parameters used for the varied parameters as well as those that were held constant.

Other aspects of the design are summarized in Table 3. A full factorial design was used with three factors and two levels ($2^3 = 8$). Two replicates for each run and two centered runs are incorporated, resulting in a total of 18 sets as shown in Table 4.

3 | RESULTS AND INTERPRETATIONS

3.1 | Hypothesis and modeling

Figure 3 schematically shows the pipe during the heating phase along with the coordinate system. The differential equation for heat conduction in the solid without heat generation expressed in 3D cylindrical coordinates and under uniform conductivity assumption, is given by[17]

$$\frac{1}{r}\frac{\partial}{\partial r}\left(r\frac{\partial T}{\partial r}\right)+\frac{\partial^2 T}{\partial x^2}+\frac{1}{r^2}\frac{\partial^2 T}{\partial \theta^2}=\frac{1}{\alpha}\frac{\partial T}{\partial t}. \quad (1)$$

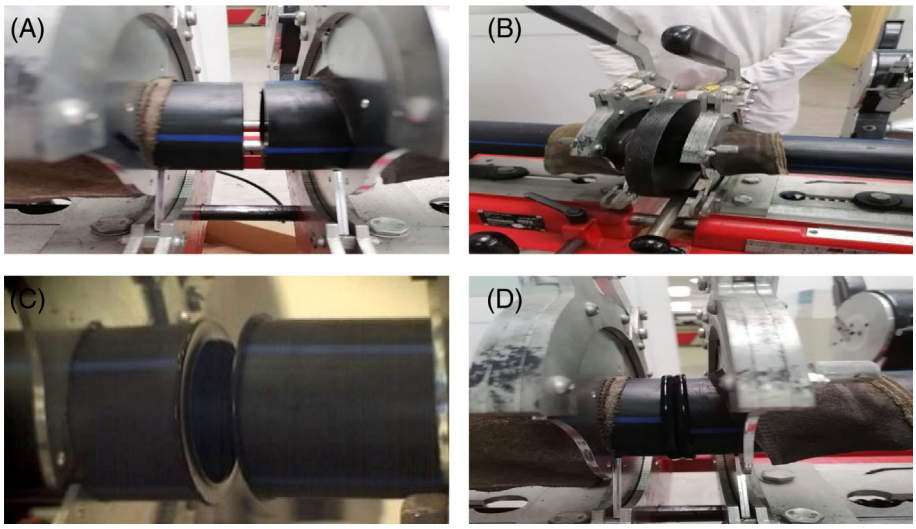

FIGURE 2 Different experimental phases of the welding process: (A) installation of the two ends of the pipes, (B) installation of a heating plate (equalization heating), (C) heating plate removal phase, and (D) welding and cooling phase.

TABLE 2 Values of test variables.

Variables		Unit	Minimum value	Center value	Maximum value
Heater plate temperature	T	°C	200	220	240
Welding and equalization force	F_1	N	110	150	190
Heating force	F_2	N	10	10	10
Equalization time	t_1	s	20	20	20
Heating duration	t_2	s	30	50	70
Plate removal time	t_3	s			5
Fusion jointing force duration	t_4	s			5
Welding and cooling duration	$t_4 + t_5$	Min			>6

TABLE 3 Design summary.

Factors	3	Base design	3; 8
Runs	16	Replicates	2
Blocks	1	Centered points (total)	2

The heat flux density in the polymers is given by Fourier's law of heat conduction:

$$q'' = -\lambda \frac{\partial T}{\partial x} \tag{2}$$

The configuration is axisymmetric, and the temperature does not depend on θ, then $T = T(x,r,t)$ and the governing equations can be written as

$$\frac{1}{r}\frac{\partial}{\partial r}\left(r\frac{\partial T}{\partial r}\right) + \frac{\partial^2 T}{\partial x^2} = \frac{1}{a}\frac{\partial T}{\partial t} \quad (ri < r < re; x > 0 \text{ and } t > 0). \tag{3}$$

Because of the limited pipe thickness (4.5 mm) and the heat transfer induced by the heating plate, the temperature dependency on radius is neglected throughout the equalization and heating phases. This assumption implies that temperature radial gradients within the solid are negligible with respect to temperature axial gradients[18] and subsequently, $T = T(x,t)$. The equalization and heating phases equation (Equation 3) is reduced to

$$\frac{\partial^2 T}{\partial x^2} = \frac{1}{\alpha}\frac{\partial T}{\partial t} \tag{4}$$

Figure 4a shows an image provided by the IR camera. Two reference lines are added L1 and L3. L1 indicates the position of transverse view line and L3 indicates the position of longitudinal view line.

Subplot 4.b shows the transverse profile of the temperature along the L1 transverse line. This profile is quasi-uniform which confirms the above-mentioned approximation. The subplot 4.c illustrates the longitudinal variation of the temperature profile. The latter is logically constant in the heating plate section and decreases in the pipe.

The assumption of Equation 4 is validated by the temperature profile plotted in Figure 4b,c. The transverse temperature profile during both the equalization and heating phases are almost constant.

During cooling phase, the temperature distribution depends on the radius and that the outer regions cool more quickly than the core of the pipe. Figure 4d demonstrates that temperature depends on radius.

To assess the temperature distribution theoretically, the appropriate form of the heat equation must be solved. General form (Equation 3) gives access to T (r, x, t) distribution during the welding-cooling phase. However, reduced form (Equation 4) allows access to T (x,t) during the heating phase. These solutions depend on the initial temporal condition as well as the physical conditions existing at the boundaries. Alternatively, temperature distribution may be determined experimentally as shown in Figure 4.

3.2 | Equalization and heating phases

3.2.1 | Temperature distribution modeling

During the equalization and heating phases, the ends of the pipes undergo heat transfer through three modes: conduction, convection, and radiation. The heat transfer propagates mainly by conduction in the x-direction, sustained by a temperature gradient along this axis. The conduction flux diminishes with increasing x coordinate, while energy conservation mandates that heat flux is dissipated to the surroundings by convection and radiation.

Figure 5 illustrates an example of the EA6 test measurements, depicting the temperature's variation over distance (X) and time (t) during the equalization and heating phases. The shape of the curves is the same as that in the work of Potente et al.[19] Additionally, heating operations in both pipe sections are conducted symmetrically. Given the symmetry of the heating plate, we only need to consider a single pipe (pipe 1).

Various mathematical expressions were evaluated to construct a suitable model capturing the relationship between temperature profile evolution and spatial–temporal variables. The most consistent agreement was achieved using the following expression:

$$\frac{T(x,t) - T_\infty}{T_0 - T_\infty} = tanh\left(B.\frac{x^{n1}}{t^{n2}}\right) \tag{5}$$

where

$T(x = 0, t) = T_0$, the heating plate temperature.

$T(x = L, t) = T_\infty$, the temperature at the free extremity of the pipe.

B, n_1, n_2 are parameters to be identified for all these tests.

The Excel Solver feature offers the ability to identify parameters for an objective function, typically denoted by a proposed formula, within a designated cell, all while conforming to specified constraints. It functions by manipulating a set of adjustable cells that represent the parameters of the objective function, modifying their

Test	Bloc	A	B	C	Fs (N)	t_{ch} (s)	T (°C)	Name
1	1	−	−	−	110	30	200	EA1-S1
2	1	+	−	−	190	30	200	EA2-S1
3	1	−	+	−	110	70	200	EA3-S1
4	1	+	+	−	190	70	200	EA4-S1
5	1	−	−	+	110	30	240	EA5-S1
6	1	+	−	+	190	30	240	EA6-S1
7	1	−	+	+	110	70	240	EA7-S1
8	1	+	+	+	190	70	240	EA8-S1
9	1	−	−	−	110	30	200	EA1-S2
10	1	+	−	−	190	30	200	EA2-S2
11	1	−	+	−	110	70	200	EA3-S2
12	1	+	+	−	190	70	200	EA4-S2
13	1	−	−	+	110	30	240	EA5-S2
14	1	+	−	+	190	30	240	EA6-S2
15	1	−	+	+	110	70	240	EA7-S2
16	1	+	+	+	190	70	240	EA8-S2
17	1	0	0	0	150	50	220	EA9-S1
18	1	0	0	0	150	50	220	EA9-S2

TABLE 4 DOE tests according to a full factorial design with two replicates and two centered points.

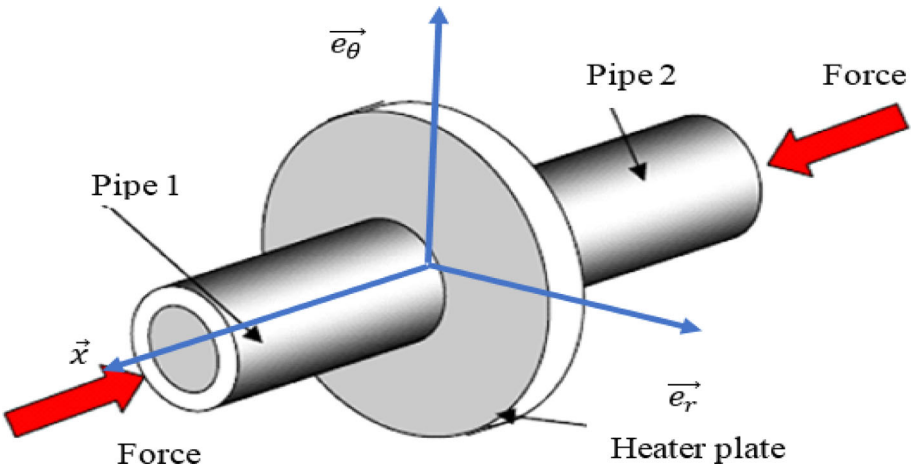

FIGURE 3 Graphic illustration of the pipe heating phase during butt welding.

values to minimize the RMSE, or Root Mean Squared Error. A lower RMSE value signifies a more accurate identification of the model parameters. The RMSE is computed at a fixed time points t_j (where $t_j \in [0, t_{ch}]$), for different positions X_i (where $X_i \in [0, Xf]$). The RMSE is computed at fixed time using the following formula:

$$(RMSE)_{t_j} = \sqrt{\frac{1}{N}\sum_{i=1}^{N}\left(T_{pred,i} - T_{exp,i}\right)^2} \qquad (6)$$

As an illustration of the outcomes, Figure 6 juxtaposes the spatial temperature profiles predicted by the baseline model with the experimental data at various time points for the EA6 test. The agreement appears to be reasonable. The corresponding identification parameters are outlined in Table 5. Specifically, for the EA6 experiment, at $x = 0, T(0,t) = T_0 = 240^{\circ}\mathrm{C}$ and the temperature at the free extremity of the pipe of $T_\infty = 41^{\circ}\mathrm{C}$.

Table 6 presents the spatial average values of RMSE for different time instants. It is evident that this error commences around 7°C, sharply escalates to 11°C during the transition from the equalization phase (softening) to the heating phase, before subsequently declining. This surge in error can be attributed to the reduction in heating force from F1 to F2, aimed at maintaining contact between the plate and the pipes, thereby explaining the observed peak in error.

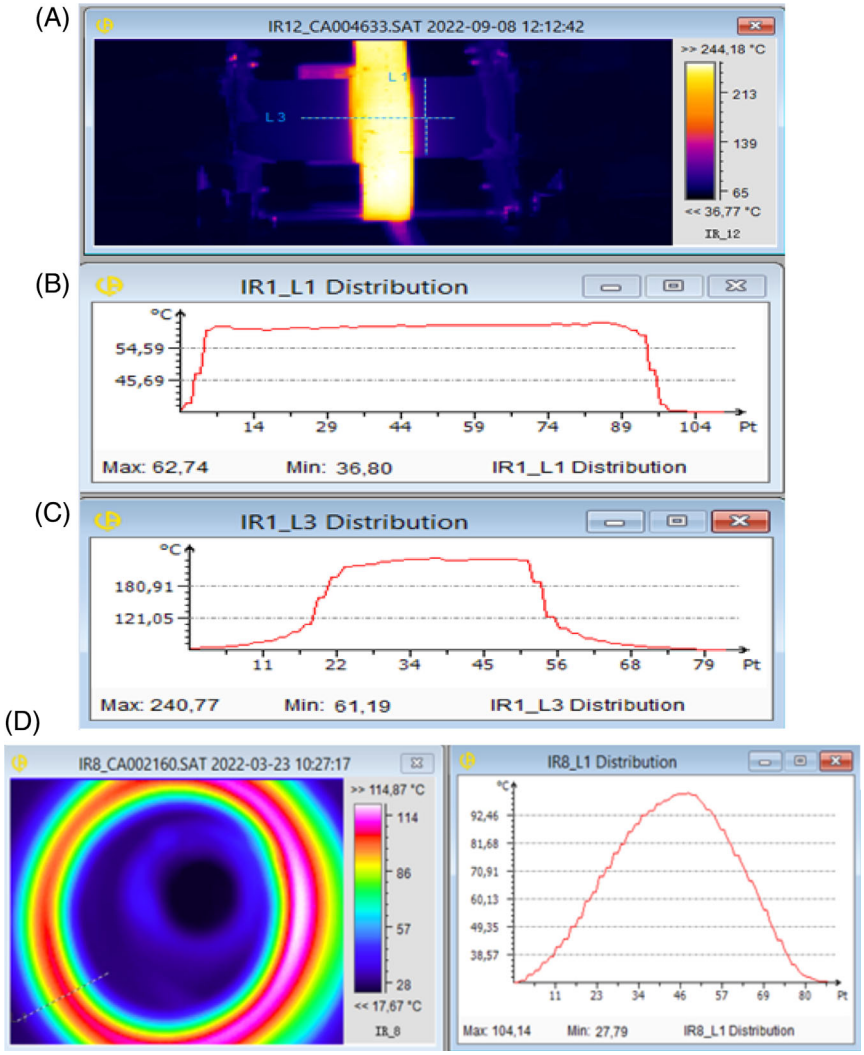

FIGURE 4 (A): IR camera image and reference lines L1 and L3. (B): Transverse temperature profile at L1 line (L1 is distant from the plate by 7 mm). (C): Longitudinal temperature profile at L3 line. (D) Circumferential infrared thermal image (left). L1-radial temperature profile (right) for the cooling phase.

A multivariate linear regression model was developed utilizing the widely employed method of ANOVA (Analysis of Variance).[20,21] The statistical analysis was executed using the software package, MINITAB.[22] The output variables were effectively modeled based on the input parameters, namely, the heating duration t_{ch}, the force Fs and the heating plate temperature T_0. The resulting regression relationships are as follows:

$$B = 209.8 - 2.781.t_{ch} \quad (7)$$

$$n1 = -5.280 + 0.03563.t_{ch} \quad (8)$$

$$n2 = -0.2486 - 0.001162.Fs \quad (9)$$

Various validation tests were conducted to assess the accuracy of the proposed general model. Table 7 provides a summary of the comparison results between the

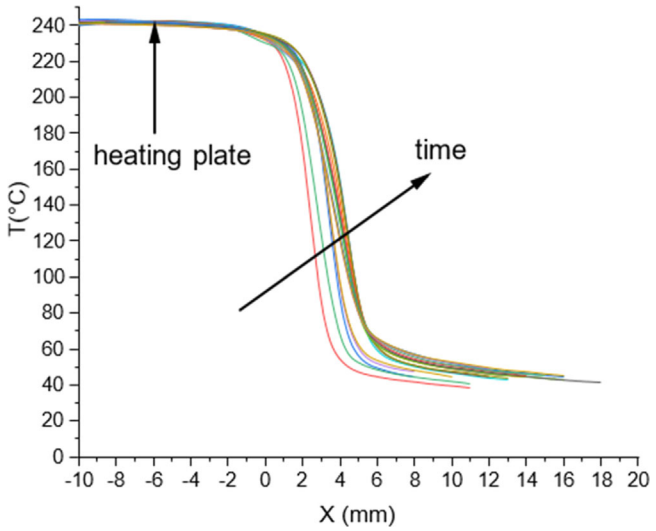

FIGURE 5 Longitudinal temperature profiles at different instants during the equalization and heating phases for pipe1.

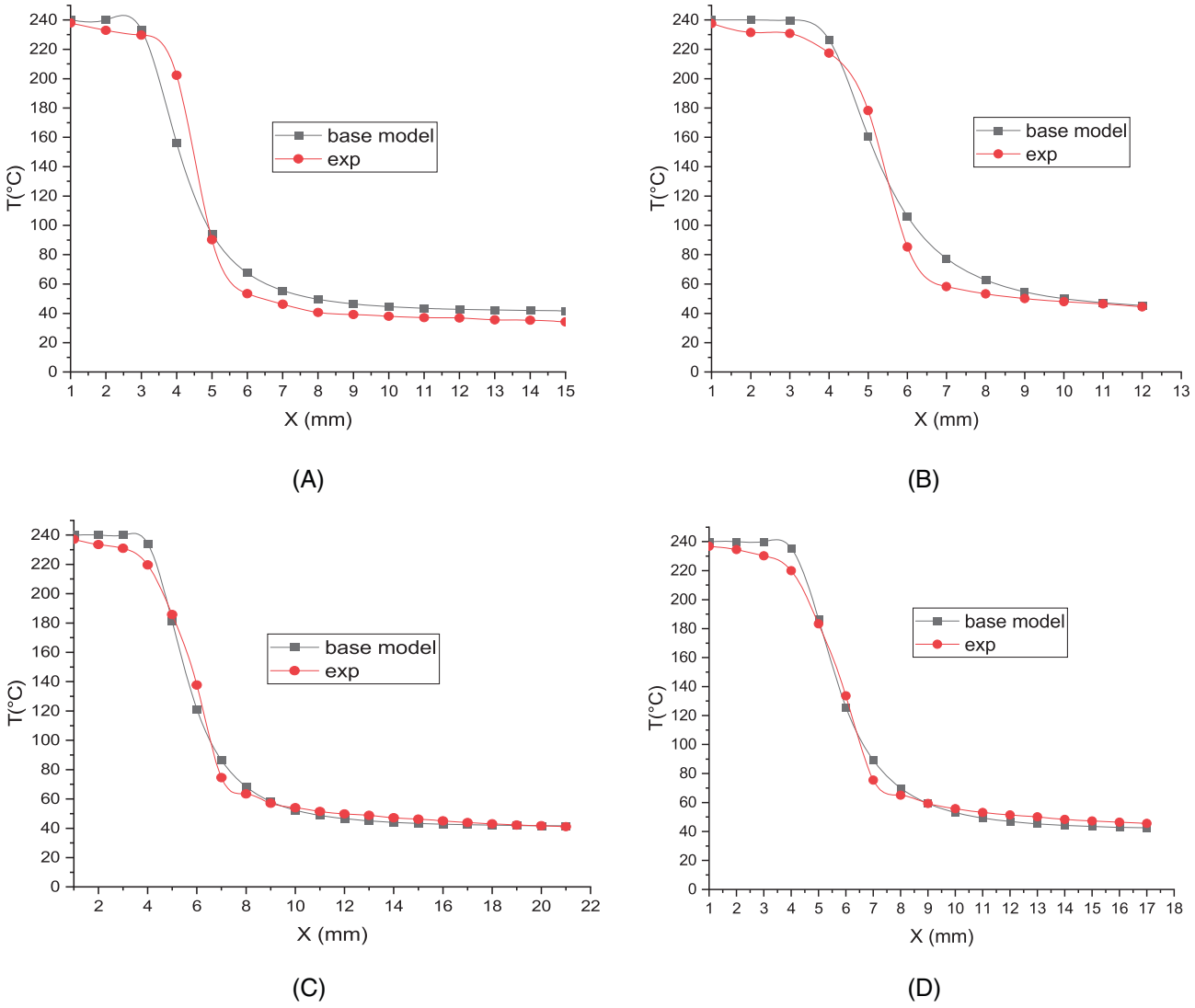

FIGURE 6 Comparison between the experimental data and the predictions obtained by the proposed model is conducted at different instants (A) $t = 3$ s, (B) $t = 22$ s, (C) $t = 36$ s, and (D) $= 41$ s.

TABLE 5 Identification of temperature relationship parameters for the EA6 test.

T_0	240°C	T_∞	41°C
B	92.743		
$n1$	−3.93	$n2$	−0.467

TABLE 6 Average error between the base model and the experimental data for the EA6 test.

Tj	$(RMSE)_{t_j}$ (°C)
$t = 3$ s	7.16
$t = 22$ s	11
$t = 36$ s	6.43
$t = 41$ s	6.79

identification parameters (B, $n1$, $n2$) of both models developed for the centered point test, EA9.

The mean errors ranged from 1.64% for the coefficient n1 to 5.8% for the coefficient B, which fall within acceptable ranges. Additionally, the relationships exhibit R^2 values exceeding 69%. These statistics indicate a satisfactory level of accuracy and reliability in the models' predictive capabilities.

3.2.2 | Melting depth modeling

By analyzing the temperature distribution during the equalization and heating phases, it becomes feasible to assess the depth of the melted zone, as depicted in Figure 7. Specifically, this depth is derived from the temperature profiles at the end of the heating duration,

TABLE 7 Comparison between the identification parameters of the general and base models at the centered point test EA9.

	B	*n*1	*n*2
Base model	75.108	−3.442	−0.4328
Multivariate model	70.75	−3.4995	−0.4229
Error	5.8%	1.67%	2.64%
R^2	79.64%	69.63%	79.2%

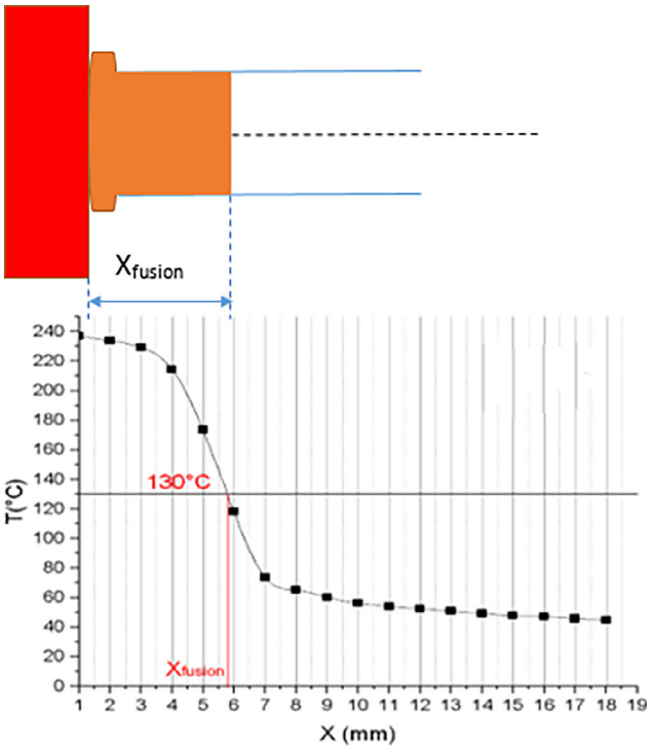

FIGURE 7 The thickness of the melt layer, X_{fusion}, determined at the end of the heating phase. It represents the distance at which the material reaches its melting temperature, typically defined as 130°C.

wherein the distance X_{fusion} is determined. X_{fusion} represents the point at which the temperature reaches the melting threshold of 130°C.[23]

The outcomes of processing various test temperature profiles are summarized in Table 8. It is noteworthy that the thickness of the melted zone increases with the increase in different parameters such as temperature, heating duration, and welding force.

For the reference case EA6, the thickness of the melt layer is measured at 6.03 mm. As the test parameters vary, the thickness of the molten layer (X_{fusion}) also varies accordingly. Once again, a statistical modeling approach

TABLE 8 Melt layer thickness for the different tests.

	Fs (N)	t_{ch} (s)	T_0 (°C)	X_{fusion} (mm)
EA1	110	30	200	5.2
EA2	190	30	200	6.1
EA3	110	70	200	5
EA4	190	70	200	7.35
EA5	110	30	240	5.1
EA6	190	30	240	6.03
EA7	110	70	240	7.75
EA8	190	70	240	8.5
EA9	150	50	220	6.4

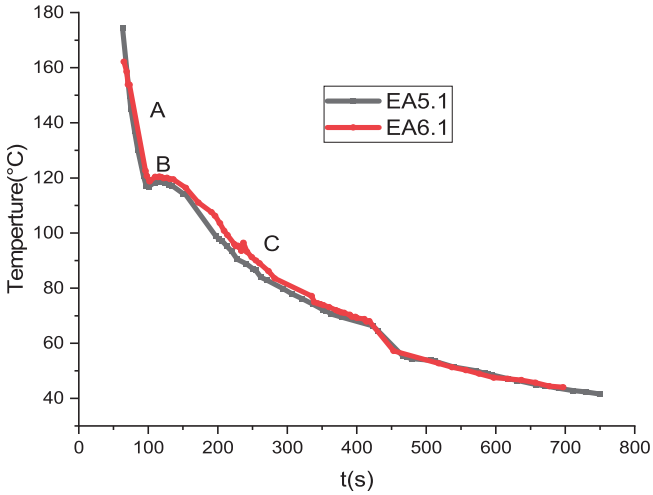

FIGURE 8 Phase change diagram of the weld joint for tests EA5 and EA6 (240°C-30 s).

TABLE 9 Summary of the identification process of the coefficients a, b, k, and n.

	A	b	K	N
EA1	−0.975	250.629	1676.04	−0.5600
EA2	−1.263	221.409	1623.148	−0.534
EA3	−0.975	250.628	4846.947	−0.706
EA4	−1.118	254.166	3205.569	−0.636
EA5	−1.760	280.483	3429.565	−0.662
EA6	−1.277	244.837	3373.905	−0.660
EA7	−1.480	317.250	1758.700	−0.509
EA8	−1.333	313.181	1149.307	−0.465
EA9	−1.118	254.166	2232.884	−0.573

is employed using MINITAB. A relationship between X_{fusion} and the input parameters Fs, t_{ch} and T_0 is established and expressed as follows:

$$X_{fusion} = 11 + 0.01541.Fs - 0.241.t_{ch} - 0.0403.T_0 + 0.001272.t_{ch}.T_0. \quad (10)$$

This model has an R^2 value of 93.24%, indicating a high degree of goodness of fit and suggesting that the proposed relationship effectively captures the variability in the melt layer thickness based on the input parameters.

Equation 11 was validated at the midpoint EA9. The predicted value is $X_{fusion} = 6.38$ mm, while experiment processing gives 6.4 mm. This demonstrates that the model accurately captures the relationship between the thickness of the molten layer (X_{fusion}) and the other parameters. The knowledge of (X_{fusion}) is invaluable for evaluating the required welding pressure (force) in each scenario to prevent complete expulsion of the molten polymer. Maintaining some material displacement at the depth of the molten zone ensures that molten polymer remains at the contact surfaces, facilitating interaction and intermolecular entanglement at the solder junction. This enhances the overall quality and strength of the bond.

3.3 | Welding and cooling phases

At the end of the heating phase, the heating plate is removed, and contact between the two extremities of the pipes is reestablished before entering the welding phase. In the absence of a heating source, temperature decreases due to heat transfer exchange with the surroundings by convection and radiation. Two distinct regions are delineated: the weld joint and the pipes. Temperature distribution is assessed for both regions.

3.3.1 | Temperature variation at a given point of the solder joint

The phase change diagram in Figure 8 illustrates the temporal evolution of the temperature in the weld joint for tests EA5 and EA6 (240°C-30 s) throughout the welding and cooling phases at a specific point within the weld joint region. Three distinct stages can be identified, each corresponding to a well-known phenomenon associated with polymer solidification.

In the first stage (A), there is a rapid linear decrease in the joint temperature down to 120°C within 100 s which correspond to 50 s since the beginning of the welding-cooling phase. Subsequently, the temperature stabilizes at a plateau (stage B), marking the onset of the solidification phase change. This plateau is maintained for a brief period, during which the temperature remains constant at 120°C. Finally, in the third stage (C), the temperature in the welding region continues to decrease over time.

The cooling curves depicted in Figure 8 closely resemble those obtained by Amanda et al.[24] They observed that a one-minute (60-s) interval is sufficient for the core temperature to decrease below the solidification and crystallization plate temperature. This time interval is contingent on various parameters such as heating temperature and time, welding force, pipe thickness, and cooling rate influenced by ambient temperature. For example, at a

TABLE 10 Comparison between coefficients identification using the model and the experience at the midpoint (the EA9 test).

Coefficient	Experience	Model	% Error
a	−1.1185	−1.2546	10.84%
b	254.169	266.645	4.68%
k	2233.88	2635	15.26%
n	−0.57329	−0.5882	2.54%

TABLE 11 Identification of the parameters of the temperature expression (18) for the EA8 test $T(x,t)$, performed using relationships between stages A and B.

a	−1.047	B	230.26
M	238925505.87	T_∞	39.71°C
m_1	−4.19	m_2	3.109

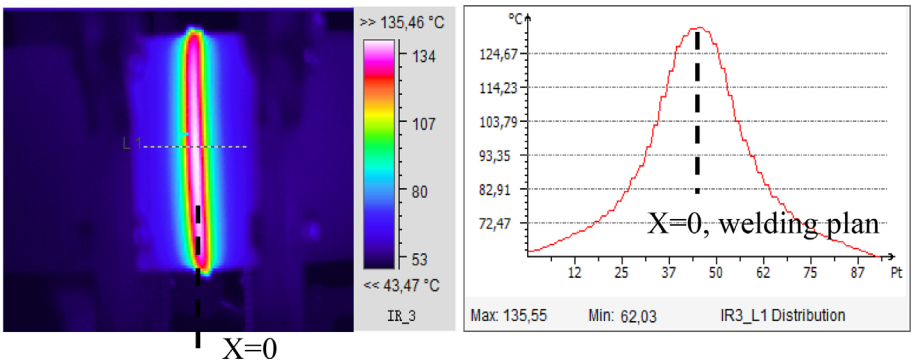

FIGURE 9 Longitudinal infrared thermal image during the welding-cooling phase.

temperature of 200°C and a heating time of 30 s, the crystallization plate lasts for 20 s, resulting in a cooling time of 50 s, which is consistent with Amanda et al.'s findings. However, at 240°C and a heating time of 70 s, the plate lasts for 60 s, leading to a cooling time of 110 s. Minimizing cooling time can be achieved by following Amanda et al.'s methodology, but specifying a more precise time for releasing welding pressure is required. In present study, in line with the DVS2207-1 standard (220°C for 50 s with a force of 150 N), the pipe clamping pressure can be released after 85 s.

The evolution of the temperature in the weld joint region can be delineated using the following mathematical expressions for the various stages:

$$\text{Stage A}: T_0(t) = a.t + b \tag{11}$$

$$\text{Stage B}: T_0(t) = 120^{\circ}\text{C} \tag{12}$$

$$\text{Stage C}: T_0(t) = k.t^n \tag{13}$$

TABLE 12 Identification of the parameters of the temperature expression (18) for the EA8 test $T(x,t)$ performed using relationships of stages C.

K	14063.24	n	−0.964
M	14,878	T_∞	38.13°C
m_1	−2.137	m_2	1.248

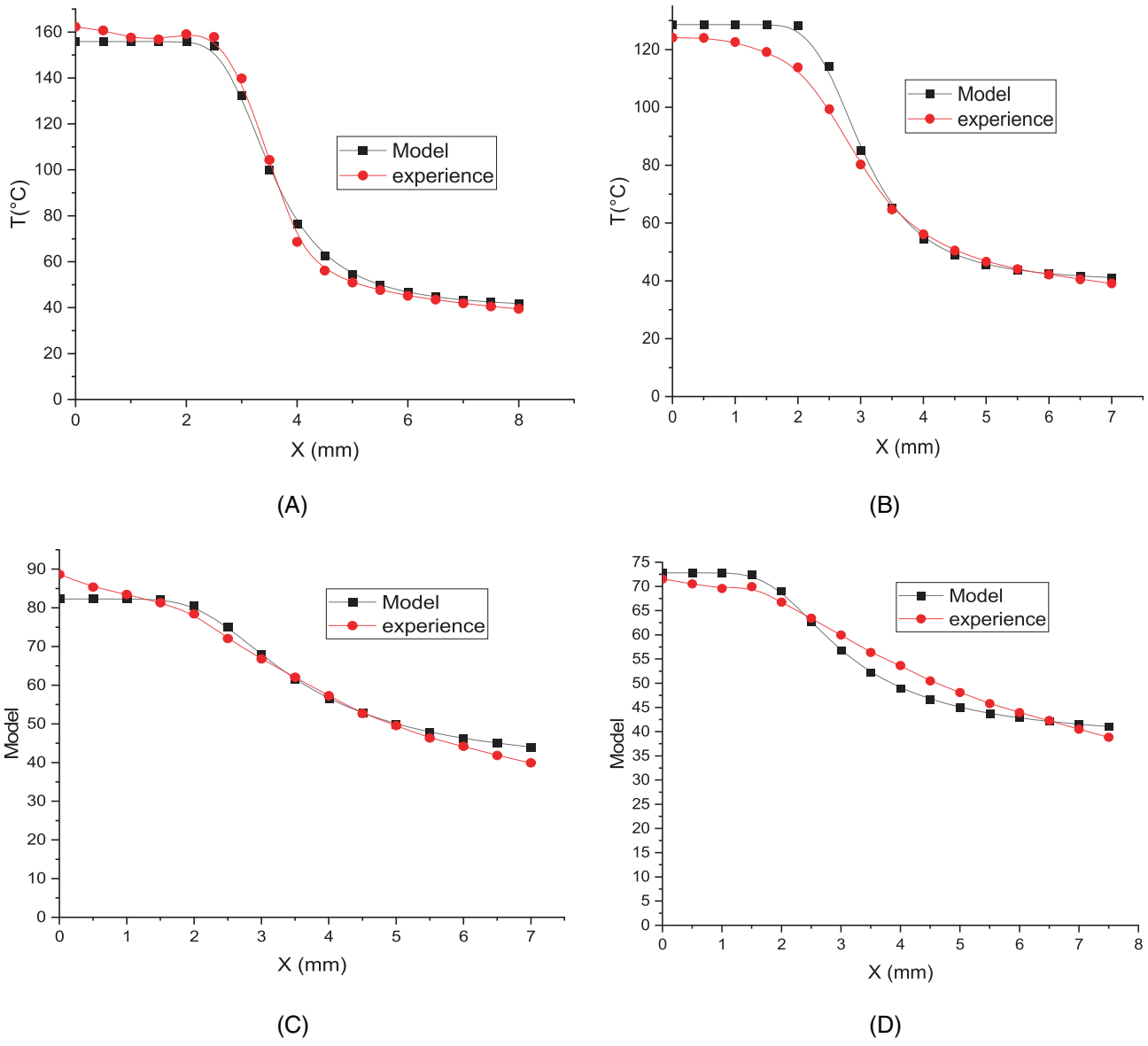

FIGURE 10 Comparison of the model results and measurements of the temperature evolution during the welding – cooling phase at different instants.

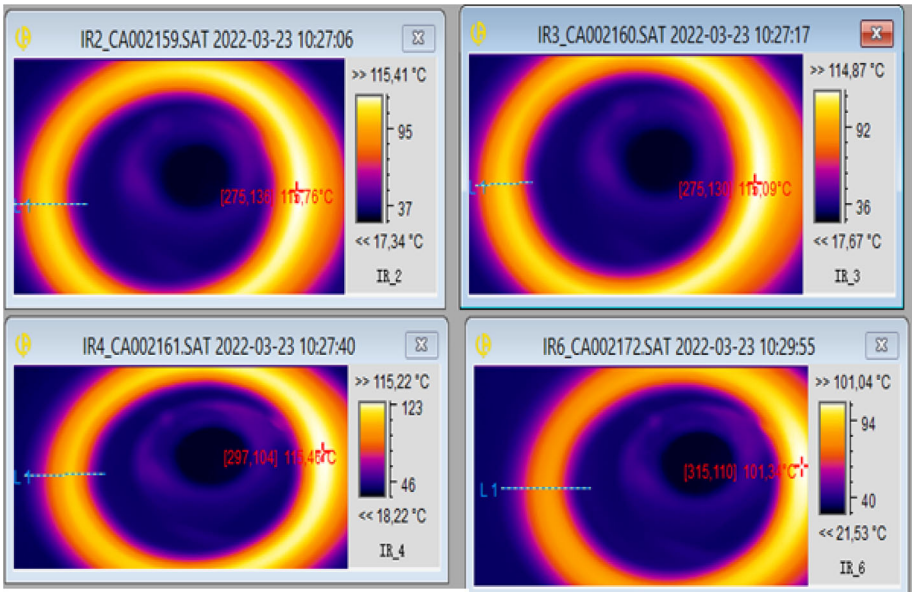

FIGURE 11 Samples of circumferential IR thermal images in welding phase.

The proposed expressions for the phase change diagram are validated for both applied temperatures during the preceding heating phase.

Table 9 presents the coefficients for the different stages of the proposed expressions governing the phase change diagram of the weld joint region, culminating in the formulation of a set of mathematical expressions for each coefficient as follows:

$$a = 6.19 - 0.0358.Fs - 0.03433.T_0 - 0.000166.Fs.T_0 \quad (14)$$

$$b = 332.2 - 0.7070.Fs - 5.621.t_{ch} - 0.012.T_0 + 0.01005.Fs.t_{ch} + 0.02261.t_{ch}.T_0 \quad (15)$$

$$k = -25110 + 600.t_{ch} + 124.9.T_0 - 2.703.t_{ch}.T_0 \quad (16)$$

$$n = 1.239 - 0.04046.t_{ch} - 0.00846.T_0 + 0.000187.T_0.t_{ch} \quad (17)$$

From the expressions of coefficients "a" and "b," we observe that stage A relies not only on the ambient temperature but also on the welding parameters and their interactions. However, for stage C, the coefficients "k" and "n" are independent of pressure (force), confirming the findings of Amanda et al.[24] that release the welding pressure after stage B (solidification plateau).

Table 10 displays the outcome of the comparison between coefficients identification using the model and empirical experience at the midpoint (the EA9 test). It provides insights on errors varying from being accepted for coefficients b and n, moderately accepted for coefficient a, and weakly accepted for coefficient k (15.26%).

R^2 values range from 86.43% for the coefficient k and 99.69% for the coefficient b.

3.3.2 | Modeling of temperature along the pipe

Figure 9 depicts the infrared thermal image of both pipes during the welding-cooling phase alongside the corresponding longitudinal temperature profile variation. The temperature profile appears symmetrical concerning the weld joint region.

The following mathematical model is derived for the temperature profiles during welding-cooling phase along the longitudinal x-dimension of the pipe:

$$\frac{T(x,t) - T_\infty}{T_0 - T_\infty} = tanh\left(M.\frac{x^{m1}}{t^{m2}}\right) \quad (18)$$

m_1 and m_2 are the model parameters.

Tables 11 and 12 display the identified coefficient for the EA8 test for the different stages of the phase change diagram.

Figure 10 illustrates the comparison between the model results and measurements for four instances during stage C for the EA8 test. The agreement is deemed satisfactory.

For assessing the radial variation of the pipe's temperature, circumferential IR images are recorded. Samples of IR images are displayed in Figure 11, indicating the presence of a significant radial temperature gradient in the pipe. The corresponding temperature profiles are shown in Figure 12.

Some findings are as follows:

- The decrease in temperature at external pipe surface (at $r = 37.5$ mm) is 15.81°C in 174 s, equivalent to a cooling rate of 5.45°C/min.

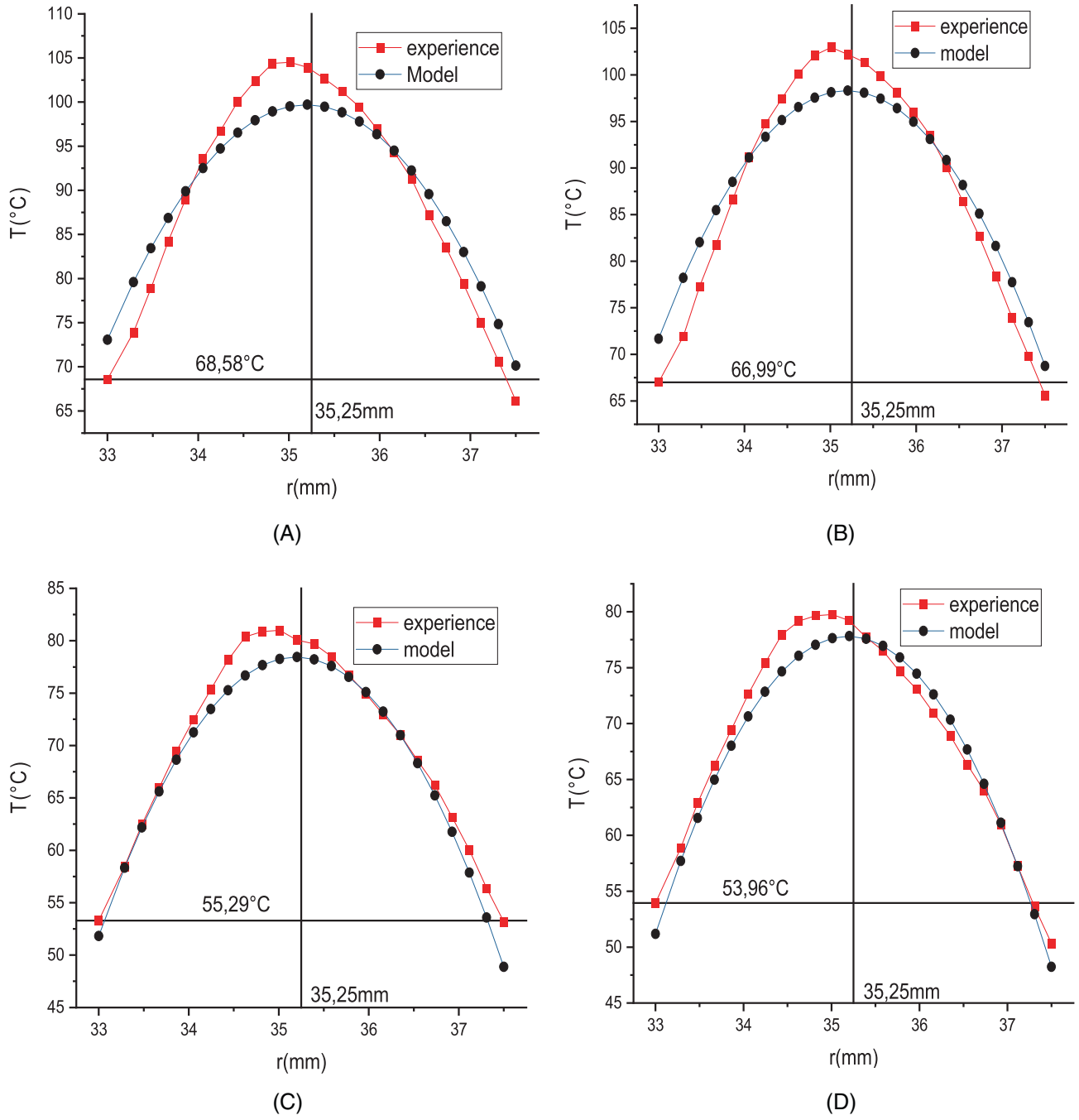

FIGURE 12 Comparison of the model results and the measurements for the radial variation at different instants (A) 289 s; (B) 300 s; (C) 458 s; and (D) 463 s.

- The decrease in temperature at internal pipe surface (at $r = 33$ mm) is 14.62°C in 174 s, resulting in a cooling rate of 5.04°C/min.
- The decrease in temperature in the middle of the pipe thickness (at $r = 35.25$ mm) is 24.74°C in 174 s, leading to a cooling rate of 8.53°C/min.

The radial variation of the temperature may be expressed as

$$T(r,t) = \left[\beta.\left(t_f - t\right) + \delta\right] + \left[I.r^2 + J.r + V\right] \text{ with } t_f = 650s \tag{19}$$

Similarly, for the heating phase, a procedure for the identification of all parameters β, δ, I, J, and V using the experimental data as input is conducted. Table 13 and Figure 12 display the results of the identification and verification processes, respectively.

TABLE 13 Identification of the parameters of the temperature expression (equation 19) for the EA8 test ($T(r,t)$).

β	0.125	δ	−16.1433
I	−5.5465	J	390.379
V	−6798.52		

Figure 12 illustrates that the radial temperature distribution follows a polynomial pattern, with the surfaces cooling down more rapidly than the core of the pipe. This phenomenon is attributed to the convective heat exchange with the surroundings.

The symmetry axis ($x = 35.25$ mm) is depicted in Figure 12 to illustrate that the maximum temperature is consistently located on the inner side of the pipe. This observation confirms that the outer side of the pipe cools more rapidly than the inner side.

4 | CONCLUSION

This study encompasses a series of experiments aimed at evaluating the influence of diverse factors on the butt-fusion welding process of Polymer Pipes. It culminates in the development of a comprehensive mathematical model that considers the combined effects and interactions of the investigated parameters. By analyzing and modeling temperature distribution and melting thickness during the equalization heating phase of the welding process, it becomes possible to regulate the welding process by predicting the molten layer's thickness based on the welding conditions. This approach minimizes heating and cooling times while maintaining acceptable quality. Furthermore, this work focuses on relatively small diameter and thin thickness to simplify the modeling of temperature distribution and molten material thickness, leveraging the linear relationship dependent on the parameters. The phase change diagram of the weld joint delineates three characteristic stages, each of which is subjected to mathematical modeling and analysis. Indeed, extending the developed methodology to larger diameters and greater thicknesses requires special consideration. As the dimensions of the pipes increase, the heat distribution and thermal gradients within the material may vary significantly. Additionally, the interaction between the welding parameters and the material properties might change, necessitating adjustments to the mathematical model.

The experimentally based predictive thermal model developed in this study for the various phases of thermomechanical butt welding holds significant practical applications in the manufacturing and processing of HDPE (PE100) products. Additionally, it significantly simplifies numerical simulations and thermomechanical coupling of the process.

DATA AVAILABILITY STATEMENT

Data supporting this study are included within the article.

ORCID

Walid Awadi https://orcid.org/0000-0002-0782-8770
Mondher Zidi https://orcid.org/0000-0002-1667-7652
Maher Ben Chiekh https://orcid.org/0000-0002-7634-6847

REFERENCES

1. Ülker A, Öztoprak N, Sayer S, Yeni C. Optimization of welding parameters of hot plate welded PC/ABS blends by using the Taguchi experimental design method. *J Elastomers Plast*. 2018; 50(2):162-181.
2. Novakovic B, Kashkoush M, ElMaraghy H. Thermal expansion of high-density polyethylene in hot plate welding applications. *Polym Eng Sci*. 2023;63(9):3173-3183.
3. Deveci S, Antony N, Nugroho S, Eryigit B. Effect of carbon black distribution on the properties of polyethylene pipes part 2: degradation of butt fusion joint integrity. *Polym Degrad Stab*. 2019;162:138-147.
4. Troughton M, Khamsehnezhad A. Short-term and long-term mechanical testing to evaluate the effect of flaws in butt fusion joints in polyethylene pipes. 2016 In Pressure Vessels and Piping Conference (Vol. 50435, p. V06BT06A050). American Society of Mechanical Engineers.
5. Gehde M, Bevan L, Ehrenstein GW. Analysis of the deformation of polypropylene hot-tool butt welds. *Polym Eng Sci*. 1992; 32(9):586-592.
6. Watson MN, Murch MG. Optimizing hot plate welding of thermoplastics. *Plast Eng*. 1989;45(6):47-49.
7. Watson MN, Murch MG. Recent developments in hot plate welding of thermoplastics. *Polym Eng Sci*. 1989;29(19):1382-1386.
8. Stokes VK. Experiments on the hot-tool welding of three dissimilar thermoplastics. *Polymer*. 1998;39(12):2469-2477.
9. Mathiyazhagan K, Singh KK, Sivabharathi V. Modeling the interrelationship between the parameters for improving weld strength in plastic hot plate welding: a DEMATEL approach. *J Elastomers Plast*. 2020;52(2):117-141.
10. Troughton MJ. *Handbook of Plastics Joining: a Practical Guide*. William Andrew; 2008.
11. Savu SV, Savu ID, Ciupitu I. Thermal analysis to evaluate ageing process in heated tool and electrofusion welding of polymer pipes. *Adv Mat Res*. 2014;837:190-195.
12. Chen H, Scavuzzo RJ, Srivatsan TS. Influence of joining on the fatigue and fracture behavior of high-density polyethylene pipe. *J Mater Eng Perform*. 1997;6:473-480.
13. Marshall JP. The influence of welding parameters on the toughness of butt fusion welds in MDPE: In *Advances in Joining Plastics and Composites, Proceedings of the International*

TWI Conference, Bradford, Yorkshire, 10-12 June 1991. Abington Publishing.

14. Troughton MJ, Hinchcliff FA. *Study of the Applicability of the Tensile Weld Test for Thick-walled Polyethylene Pipe*. Vol 1. Society of Plastics Engineers; 1997:1214-1217.
15. Vlachopoulos J, Strutt D. Basic heat transfer and some applications in polymer processing. *Plastics Technician's Toolbox*. Vol 2. Society of Plastics Engineers; 2002:21-33.
16. DeCoursey W. *Statistics and Probability for Engineering Applications*. Elsevier; 2003.
17. Bergman TL, Lavine AS, Incropera FP, DeWitt DP. *Introduction to Heat Transfer*. John Wiley & Sons; 2011.
18. Wood AS. The butt-fusion welding of polymers. *Chem Eng Sci*. 1993;48(17):3071-3082.
19. Potente H, Tappe P. Heated tool-butt welding of polyethylene-pipes—welding parameters and testing technique. *Mater Des*. 1984;5(6):273-280.
20. Sharma GVSS, Rao RU, Rao PS. A Taguchi approach on optimal process control parameters for HDPE pipe extrusion process. *J Industr Eng Int*. 2017;13:215-228.
21. Raouache E, Boumerzoug Z, Rajakumar S, Khalfallah F. Effect of FSW process parameters on strength and peak temperature for joining high-density polyethylene (HDPE) sheets. *Revue Des Compos Des Matér Adv*. 2018;28(2):149-160.
22. Tashkandi MA, Becheikh NM. Optimization of joining HDPE rods by continuous drive friction welding. *Mater Sci-Pol*. 2022;40(2):240-256.
23. Cai Z, Dai H, Fu X. Investigation on the hot melting temperature field simulation of HDPE water supply pipeline in gymnasium pool. *Results Phys*. 2018;9:1050-1056.
24. Hawkins A, Engineer MT. Increasing HDPE butt fusion productivity by optimizing the cool time based on thermal mass characteristics without compromising joint strength. *Art Ther*. 2018;12:24-26.

How to cite this article: Awadi W, Zidi M, Ben Chiekh M. An experimental-based thermal prediction model for butt fusion welding of polymer pipes. *Polym Eng Sci*. 2024;1-15. doi:10.1002/pen.26781